Coupling between Voltage Sensors and Activation Gate in Voltage-gated K^+ Channels

Zhe Lu, Angela M. Klem, and Yajamana Ramu

Department of Physiology, University of Pennsylvania, Philadelphia, PA 19104

ABSTRACT Current through voltage-gated K^+ channels underlies the action potential encoding the electrical signal in excitable cells. The four subunits of a voltage-gated K^+ channel each have six transmembrane segments (S1–S6), whereas some other K^+ channels, such as eukaryotic inward rectifier K^+ channels and the prokaryotic KcsA channel, have only two transmembrane segments (M1 and M2). A voltage-gated K^+ channel is formed by an ion-pore module (S5–S6, equivalent to M1–M2) and the surrounding voltage-sensing modules. The S4 segments are the primary voltage sensors while the intracellular activation gate is located near the COOH-terminal end of S6, although the coupling mechanism between them remains unknown. In the present study, we found that two short, complementary sequences in voltage-gated K^+ channels are essential for coupling the voltage sensors to the intracellular activation gate. One sequence is the so called S4–S5 linker distal to the voltage-sensing S4, while the other is around the COOH-terminal end of S6, a region containing the actual gate-forming residues.

KEY WORDS: Shaker • DRK1 • KcsA • S4-S5 linker • S6

INTRODUCTION

Outward currents through voltage-gated K^+ channels underlie the action potentials that encode the electrical signal in nerve, muscle, and endocrine cells. A voltage-gated K^+ channel consists of four subunits, each containing six transmembrane segments (S1–S6) (Tempel et al., 1987; Kamb et al., 1988; Pongs et al., 1988; MacKinnon, 1991). In contrast, each of the four subunits in eukaryotic inward-rectifier K^+ channels or the prokaryotic KcsA channel contains only two transmembrane segments (M1 and M2) (Ho et al., 1993; Kubo et al., 1993; Schrempf et al., 1995; Yang et al., 1995; Cortes and Perozo, 1997; Heginbotham et al., 1997; Doyle et al., 1998). A voltage-gated channel is formed by an ion-pore module (S5–S6, approximately equivalent to KcsA's M1–M2) and the surrounding voltage-sensing modules (Kubo et al., 1993; Li-Smerin and Swartz, 1998; Lu et al., 2001). The atomic structure of the KcsA pore has been determined by X-ray crystallography, showing how the K^+ selectivity filter is formed by the signature sequence within the region between M1 and M2 while the remaining part of the pore is lined by M2, and how the structure gives rise of K^+ conduction (Doyle et al., 1998; Morais-Cabral et al., 2001; Zhou et al., 2001).

The S4 segments have a high density of positively charged residues. A large set of studies support the idea that S4 segments function as the primary voltage sensors (e.g., Papazian et al., 1991; Liman et al., 1991; Perozo et al., 1994; Yang and Horn, 1995; Aggarwal and MacKinnon, 1996; Mannuzzu et al., 1996; Seoh et al., 1996; Yang et al., 1996; Larsson et al., 1996; Cha et al., 1999; Glauner et al., 1999). Mutations in S4 affect channel gating, and neutralizing certain positively charged residues in S4 reduces the number of gating charges in a channel. The extracellular versus intracellular accessibility of cysteine, substituting for the positive charged residues, varies with membrane voltage. Fluorescence-based studies show that S4 undergoes conformational changes upon changing membrane voltage.

The activation gate in voltage-gated K^+ channels is located at the intracellular end of the pore (Armstrong, 1971; Holmgren et al., 1997). The pattern of state-dependent accessibility of substituting cysteine and other scanning mutagenesis studies locate the gate at the intracellular end of S6, which is also supported by EPR studies in KcsA (Liu et al., 1997; Holmgren et al., 1998; Perozo et al., 1999; del Camino et al., 2000; del Camino and Yellen, 2001; Hackos et al., 2002). A recent comparative study of a closed-state structure of KcsA versus an open-state structure of a Ca^{2+}-gated K^+ channel provides insight into the issue of how the gate-forming elements move toward, and away from, the central axis of the pore during channel gating (Jiang et al., 2002a,b).

In the case of the Shaker voltage–gated K^+ channel, the channel gate appears to be coupled tightly to the voltage sensors. The voltage dependence of Shaker's open probability (P_O) is undiminished even when it reaches as low as $\sim 10^{-7}$ at a negative voltage, and no voltage-independent channel opening was observed

Address correspondence to Dr. Zhe Lu, University of Pennsylvania, Department of Physiology, D302A Richards Building, 3700 Hamilton Walk, Philadelphia, PA 19104. Fax: (215) 573-1940; E-mail: zhelu@mail.med.upenn.edu

(Islas and Sigworth, 1999). Thus far, the coupling mechanism between the voltage sensors and the channel gate remains unknown.

We previously made a chimera between Shaker and KcsA in which Shaker's S5 through S6 is replaced by its counterpart in KcsA (Lu et al., 2001). The chimera remains voltage sensitive and K^+ selective. Thus, the transplanted KcsA pore appears to be gated by Shaker's machinery. Another study shows that a Shaker-KcsA chimera lacking Shaker's COOH terminus does not conduct any current even though it reaches the membrane (Caprini et al., 2001), because the proximal part of the COOH terminus is essential (VanDongen et al., 1990; Hoshi et al., 1991). Based on these findings, we suggested that the mechanical coupling between the voltage sensors and the intracellular activation gate primarily involves the interactions between the so called S4-S5 linker and the region around the COOH-terminal end of the S6 (Lu et al., 2001). A recent study also suggests that an interaction between some residues in these two regions underlies the coupling in the HERG K^+ channel (Tristani-Firouzi et al., 2002). In the present study, we set out to delineate the regions in the Shaker voltage-gated K^+ channel that are essential for coupling the channel gate to the voltage sensors.

MATERIALS AND METHODS

Molecular Biology and Oocyte Preparation

The cDNA of Shaker H4 with N-type inactivation removed (6–46; Shaker-IR) was subcloned in the pGEM-HESS plasmid, whereas the cDNA of DRK1 (Kv2.1) was subcloned in a pBluescript plasmid which contains seven mutations in the P-region (DRK1-Δ7) conferring AgTx2 sensitivity (Kamb et al., 1988; Frech et al., 1989; Hoshi et al., 1990; Aggarwal, 1996). For presentation purposes, we will simply refer to Shaker-IR and DRK1-Δ7 as Shaker and DRK1. The KcsA pore sequence contains mutations Q58A, T61S, and R64D conferring AgTx2 sensitivity (MacKinnon et al., 1998). All mutant cDNAs were obtained through PCR-based mutagenesis and confirmed by DNA sequencing. The cRNAs were synthesized with T7 polymerase (Promega) using linearized cDNA as templates. Oocytes harvested from *Xenopus laevis* (*Xenopus* One) were incubated in a solution containing NaCl, 82.5 mM; KCl, 2.5 mM; $MgCl_2$, 1.0 mM; HEPES (pH 7.6), 5.0 mM; and collagenase, 2–4 mg/ml. The oocyte preparation was agitated at 80 rpm for 60–90 min. It was then rinsed thoroughly and stored in a solution containing NaCl, 96 mM; KCl, 2.5 mM; $CaCl_2$, 1.8 mM; $MgCl_2$, 1.0 mM; HEPES (pH 7.6), 5 mM; and gentamicin, 50 μg/ml. Defolliculated oocytes were selected and injected with RNA at least 2 and 16 h, respectively, after collagenase treatment. All oocytes were stored at 18°C.

Recordings and Solutions

Whole oocyte currents were recorded using a two-electrode voltage-clamp amplifier (Warner OC-725C), filtered at 1 kHz, and sampled at 5 kHz using an analogue-to-digital converter (Digi-Data 1200; Axon Instruments, Inc.) interfaced with a personal computer. pClamp6 software (Axon Instruments, Inc.) was used to control the amplifier and acquire the data. The resistance of electrodes filled with 3 M KCl was ~0.3 MΩ. All currents were recorded as the membrane potential was stepped from the −80-mV holding potential to various test potentials between −80 and 80 mV in 10-mV increments and then to −50 mV for Figs. 1, B and E, and 2, B and C, but to −100 mV elsewhere in the study. All current records were corrected for background leak currents using the current templates obtained in the presence of synthetic AgTx2 at concentrations $>100 \times K_d$, except when showing no current expression for some constructs in Figs. 1 and 6 (Garcia et al., 1994). Microscopic currents were recorded from cell-attached membrane patches of *Xenopus* oocytes with an Axopatch 200B amplifier (Axon Instruments, Inc.), filtered at 1 kHz, and sampled at 5 kHz. All current records were corrected for background leak currents with a trace without open channel activity. The resistance of the patch pipette filled with the recording solution is ~3 MΩ. During current recording, the voltage across the membrane patch was stepped from the −80 mV holding potential to 80 mV and then to −100 mV. The bath solution in all recordings and the pipette solution in patch recordings contained (in mM): 100 K^+ (Cl^- + OH^-), 0.3 $CaCl_2$, 1 $MgCl_2$, and 10 HEPES; pH was adjusted to 7.6 with KOH. A mixture of hanatoxins (HaTx) 1 and 2 was purified from the venom of *Grammostola spatulata* as described previously (Swartz and MacKinnon, 1995). The mass of purified materials determined on a mass spectrophotometer corresponds to those of HaTx1 and HaTx2. For presentation purposes, we will simply refer to the two toxins together as HaTx.

RESULTS

Delineating the Essential Region in S6 through the Beginning of the COOH Terminus

Fig. 1 A compares the sequence of S6 and its distal extension among four classic voltage-gated K^+ channels. The conservation among the sequences ends at the tyrosine residue indicated by the arrow. To delineate the distal boundary of the critical region within the shown Shaker sequence, we made several mutants lacking certain COOH-terminal residues under the horizontal bar. A mutant that lacks the HRE residue trio after the conserved tyrosine still conducts voltage-gated K^+ currents, albeit with significantly altered gating properties (Fig. 1 B, E, and H). The gating property of the HRE deletion mutant is similar to Shaker containing a single mutation, L398W (Li-Smerin et al., 2000). In contrast, mutants that lack the preceding NFN, YFY, or other combinations of residues do not express current (Fig. 1 C, D, F, and G). These findings directed our investigation to the conserved region proximal to the deletable HRE.

Fig. 2 A shows schema of the polypeptide chain topology of a Shaker-KcsA chimeric channel subunit and partial sequences of the parent channels around the splicing sites. As indicated by the pair of arrows, the proximal junction in the chimera is formed between Shaker's L396 and KcsA's G30, connecting Shaker's S4–S5 linker to KcsA's M1, whereas the distal junction is between KcsA's L105 and Shaker's P473. For structural reference, the replacing KcsA sequence is shown in blue ribbon in Fig. 11 (Zhou et al., 2001). Fig. 2 B shows currents of Shaker recorded in the presence of

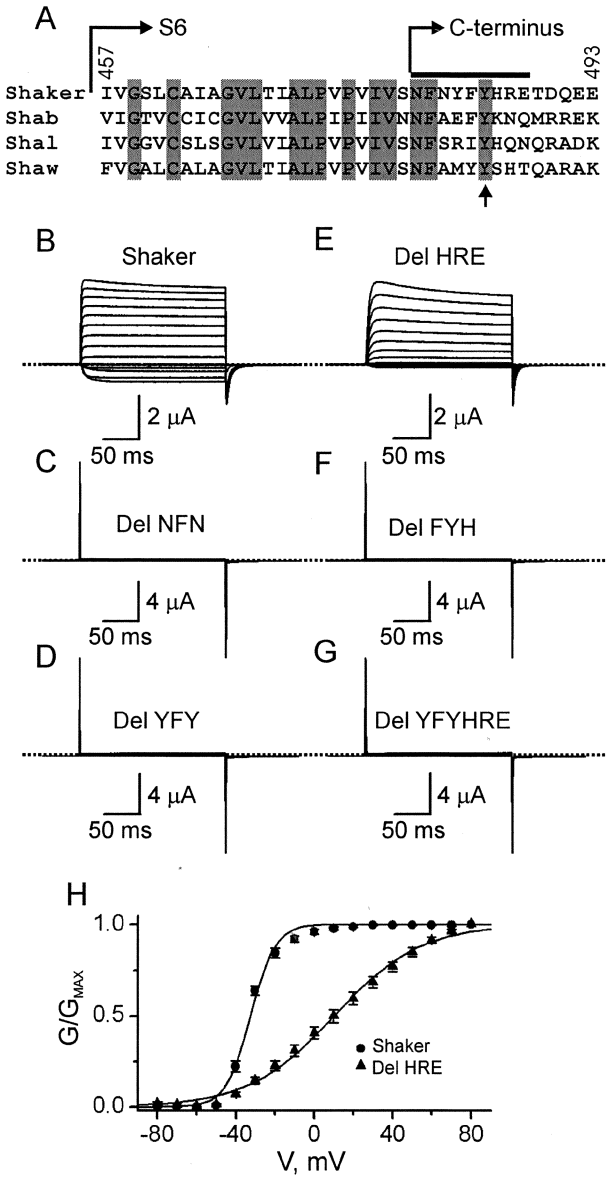

FIGURE 1. Deletions of COOH-terminal residues in Shaker. (A) Sequence alignment of S6 and initial part of the COOH terminus for four voltage-gated K^+ channels (the arrow indicates the last conserved residue in the region). (B–G) Current records from oocytes injected with RNA encoding Shaker or mutants that lack the indicated residues in the region under the horizontal bar in A. Dotted lines identify the zero current level. (H) G-V curves for Shaker and the HRE deletion mutant; the data points represent mean currents (± SEM, n = 15 and 6). The fitted curves correspond to the Boltzmann function, yielding $V_{1/2} = -32.8 \pm 0.3$ mV and valence (Z) = 3.9 ± 0.3 for Shaker, and $V_{1/2} = 6.8 \pm 1.3$ mV (n = 6) and Z = 1.1 ± 0.1 for the HRE deletion mutant.

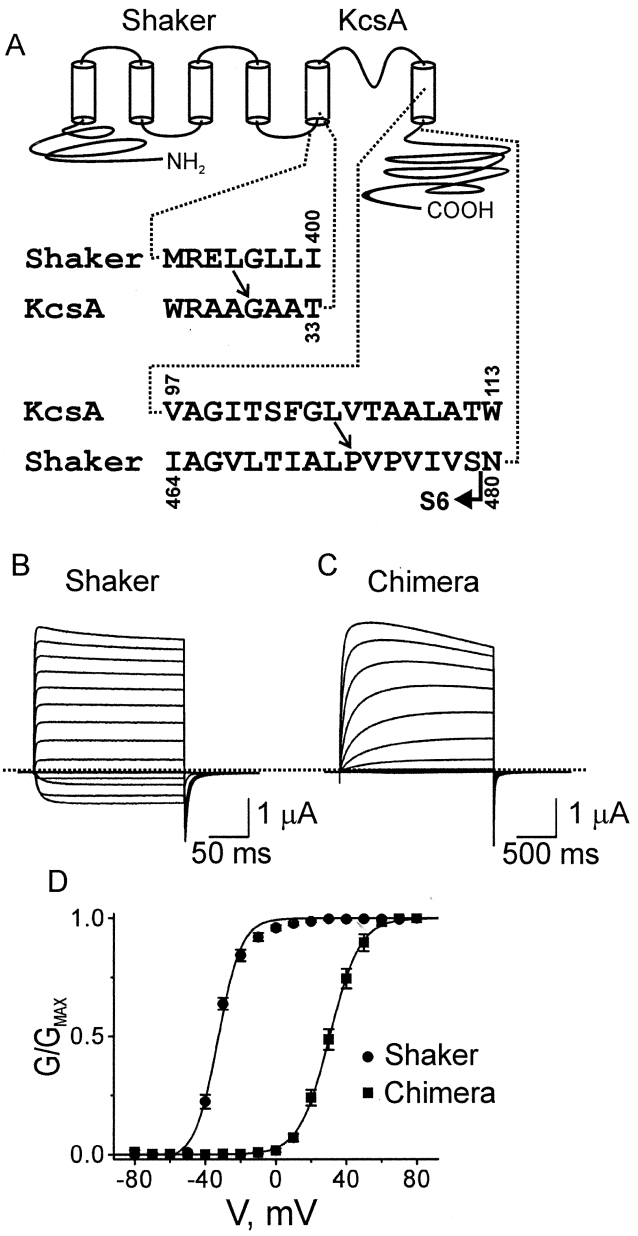

FIGURE 2. Comparison between Shaker and a Shaker-KcsA chimera. (A) Schema of the polypeptide chain topology of a Shaker-KcsA chimeric channel subunit and partial sequences of the parent channels around the splicing sites. (B–D) Currents of Shaker (B) and the chimera (C), and the corresponding G-V curves (D) where the data points represent mean currents (± SEM; n = 9 and 15). The fitted curves superimposed on the data correspond to the Boltzmann function, yielding $V_{1/2} = -32.8 \pm 0.3$ mV and valence (Z) = 3.9 ± 0.3 for Shaker, and $V_{1/2} = 30.5 \pm 0.3$ mV and Z = 3.0 ± 0.1 for the chimera.

100 mM extracellular K^+. Membrane depolarization activates the channels whereas hyperpolarization deactivates them. At the −80 mV holding potential Shaker does not conduct any detectable current. Fig. 2 C shows the current records from the Shaker-KcsA chimera in which Shaker's S5 through most of S6 is replaced by its counterpart in KcsA, as depicted in Fig. 2 A. Like Shaker, the chimeric construct does not conduct any detectable current at −80 mV. The midpoint of the G-V curve for the chimera is significantly right shifted, whereas the apparent valence is a little reduced (Fig. 2 D). In contrast, as we showed previously, another chi-

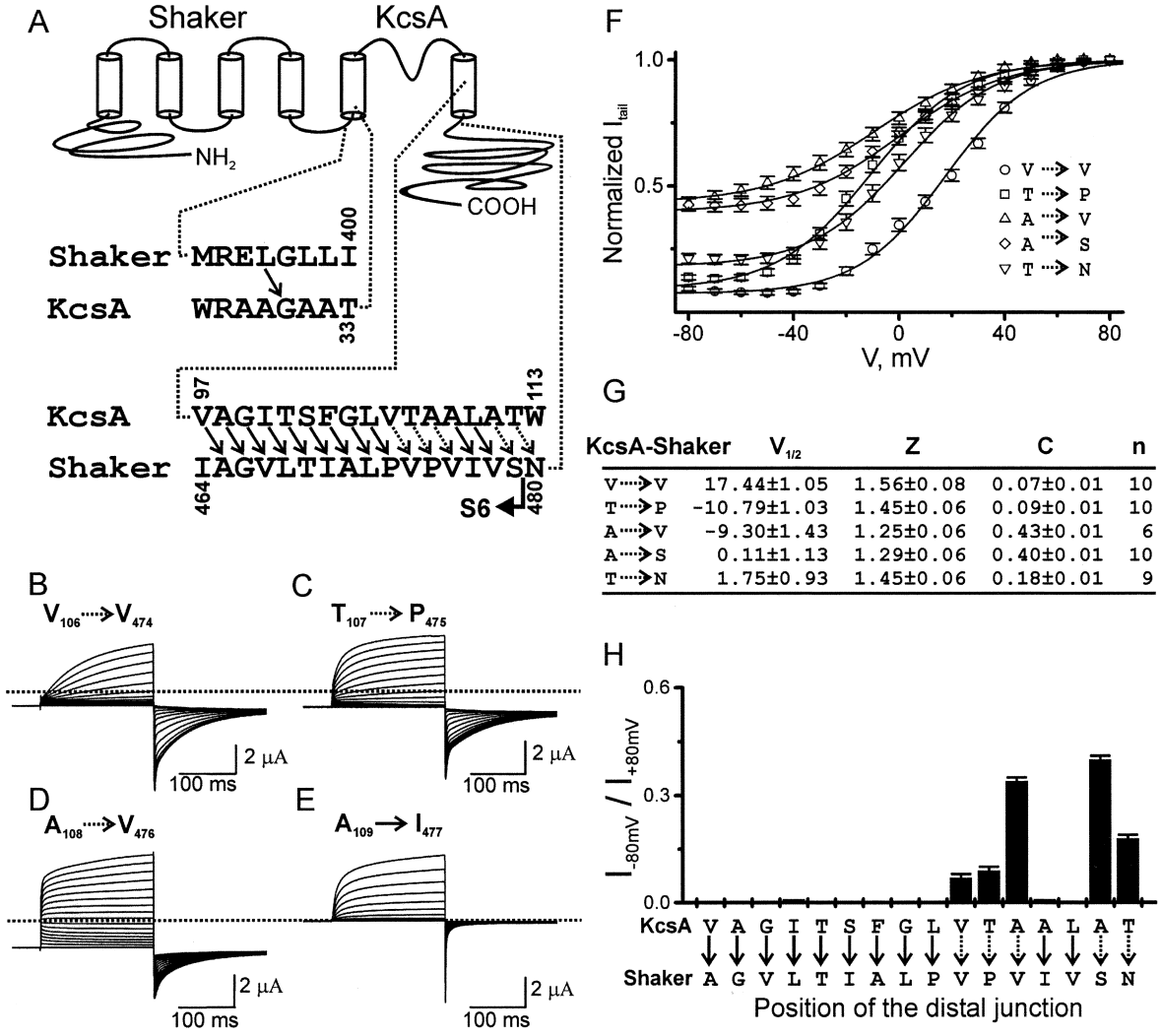

FIGURE 3. Shaker-KcsA chimeras with various distal junctions in S6. (A) Schema of the polypeptide chain topology of a Shaker-KcsA chimeric channel subunit and partial sequences of the parent channels around the splicing sites. All chimeras have the same proximal junction connecting Shaker's L396 to KcsA's G30 as indicated by the arrow. The distal junction is varied across the region, as pictured by the arrows, where the arrow type indicates whether a chimera expresses minimal (solid) or robust (dotted) voltage-independent conductance. (B–E) Current records of chimeric channels with the distal junction at four consecutive positions. (F) G-V curves (normalized tail currents vs. membrane voltage) for all chimeras expressing voltage-independent conductance at negative voltage. The fitted curves correspond to the Boltzmann function with an extra constant, "C," which accounts for the voltage-independent conductance at negative voltage. (G) Values of $V_{1/2}$ (mean ± SEM), Z, and C from the fits in F, where n is the number of oocytes examined. (H) The ratio (mean ± SEM, n = 5–11) of the currents at −80 and 80 mV versus the position of the distal junction in the chimeric constructs.

mera with a distal junction at the end of S6 (between KcsA's T112 and Shaker's N480) exhibits voltage-independent conductance at negative voltage, i.e., the macroscopic current cannot be reduced to a nondetectable level with hyperpolarization (Lu et al., 2001).

To determine the essential Shaker sequences that must be preserved for the channels to be fully gated such that the conductance of the channels can be reduced to the minimum with hyperpolarization, we gradually increased the length of the replaced S6 sequence by moving the distal junction in the chimera, one residue at a time, along the distal 2/3 of S6 (Fig. 3 A). All chimeras have an identical proximal junction (Shaker's L396–KcsA's G30) connecting Shaker's S4–S5 linker to KcsA's M1, as in Fig. 2, A and C. Fig. 3, B–E, shows representative current records from chimeras with four consecutive distal junctions. Although all four constructs are gated by voltage, three of the chimeric channels express apparently voltage-independent conductance at negative voltage, a property they share with Shaker mutant P475D (Hackos and Swartz, 2001; Hackos et al., 2002). At negative voltages the G-V curve of

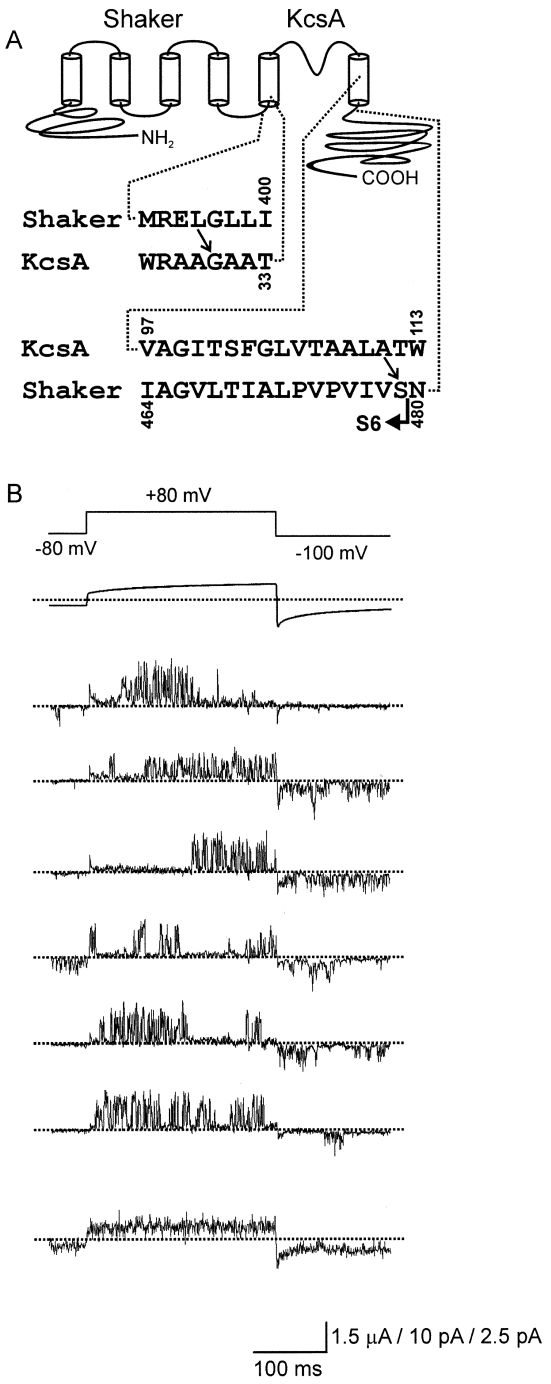

FIGURE 4. Currents of Shaker-KcsA chimeric channels recorded from a membrane patch versus a whole oocyte. (A) Schema of the polypeptide chain topology of a Shaker-KcsA chimeric channel subunit and partial sequences of the parent channels around the splicing sites. (B) Current records of the chimera. The first trace, below the voltage protocol, was recorded from a whole oocyte with a two-electrode voltage-clamp amplifier. The next six traces were recorded with a patch-clamp amplifier from a cell-attached patch, whereas the last one is the ensemble average of 50 current traces.

the chimeras approaches a constant nonzero value characteristic for a given chimera (Fig. 3 F). In contrast, as in the case of Shaker, the G-V curve of the fully gated chimeras approaches zero; an example of the latter has been shown in Fig. 2, C and D. The chimeras expressing voltage-independent conductance at negative voltage enter the closed state and exhibit a reduced open probability at negative voltage, as shown with the chimera whose distal junction is near the end of S6 between KcsA's A111 and Shaker's S479 (Fig. 4). This finding indicates that the voltage-independent conductance at negative voltage does not result from the gate becoming leaky. The voltage-independent conductance at negative voltage occurs when Shaker's four residue PVPV sequence is partially (but not when fully) replaced by its counterpart from KcsA, or when the distal junction occurs at the end of S6 (Fig. 3, A and H). Thus, the conserved PVPV sequence is apparently not absolutely required for voltage gating. Some possible functional significance of the sequence has been discussed previously (del Camino et al., 2000; del Camino and Yellen, 2001; Lu et al., 2001; Hackos et al., 2002; Jiang et al., 2002b). The present results are consistent with the scenario that some special structural features of PVPV may favor certain interactions of S6 with its neighbors and therefore strengthen the coupling between voltage sensors and the channel gate. For later reference, we colored part of KcsA's M2 red in the structural model, delineating the region that contains the residues at the varied distal junction in the chimeric channels expressing voltage-independent conductance at negative voltage (Fig. 11).

Upon depolarization, the Shaker channel has to travel through multiple closed states to reach the open state. Consequently, the time course of the current onset upon depolarization is not single exponential but sigmoidal. This feature of Shaker is preserved in the chimeric channels. For example, Fig. 5 B shows the current records of a chimera whose distal junction is between KcsA's L110 and Shaker's V478, and therefore does not contain the conserved PVPV sequence (Fig. 5 A). Despite this, the chimera remains fully gated by voltage. A set of current records of the chimera with higher temporal resolution are shown in Fig. 5 C, where there is a clear delay between the beginning of the depolarizing voltage pulse (indicated by the arrow) and the onset of the current, resulting in a sigmoidal time course. Therefore, as in Shaker, activation of the chimera is also limited by more than one transition.

Without additional compensating mutations, moving the junction beyond S6 into the COOH terminus tends to render chimeras expressing no current. For example, a construct with the distal junction connecting KcsA's E118 to Shaker's H486 does not conduct (Fig. 6, A and D). Fig. 6 B shows an alternative alignment with a triple-residue gap in the KcsA sequence. Three constructs based on that alignment also do not conduct, regardless of whether their junction is between KcsA's

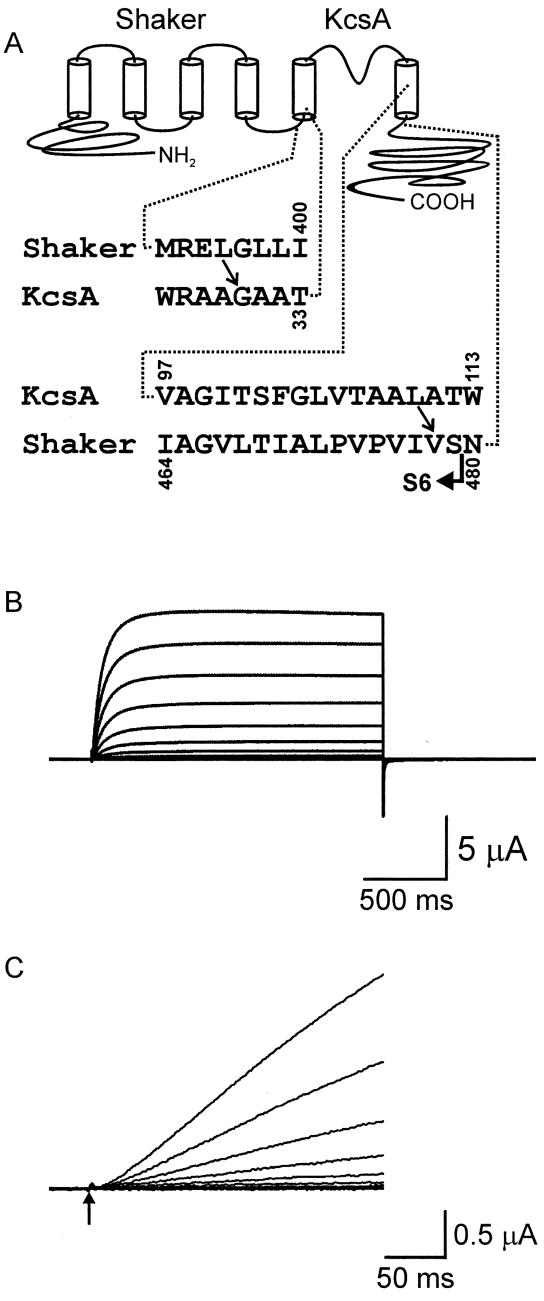

FIGURE 5. Time course of the current onset in chimeric channels. (A) Schema of the polypeptide chain topology of a Shaker-KcsA chimeric channel subunit and partial sequences of the parent channels around the splicing sites. (B) Current traces of the chimeric channels, whose initial part is shown in higher temporal resolution in C, where the beginning of the depolarization pulses is indicated by the arrow.

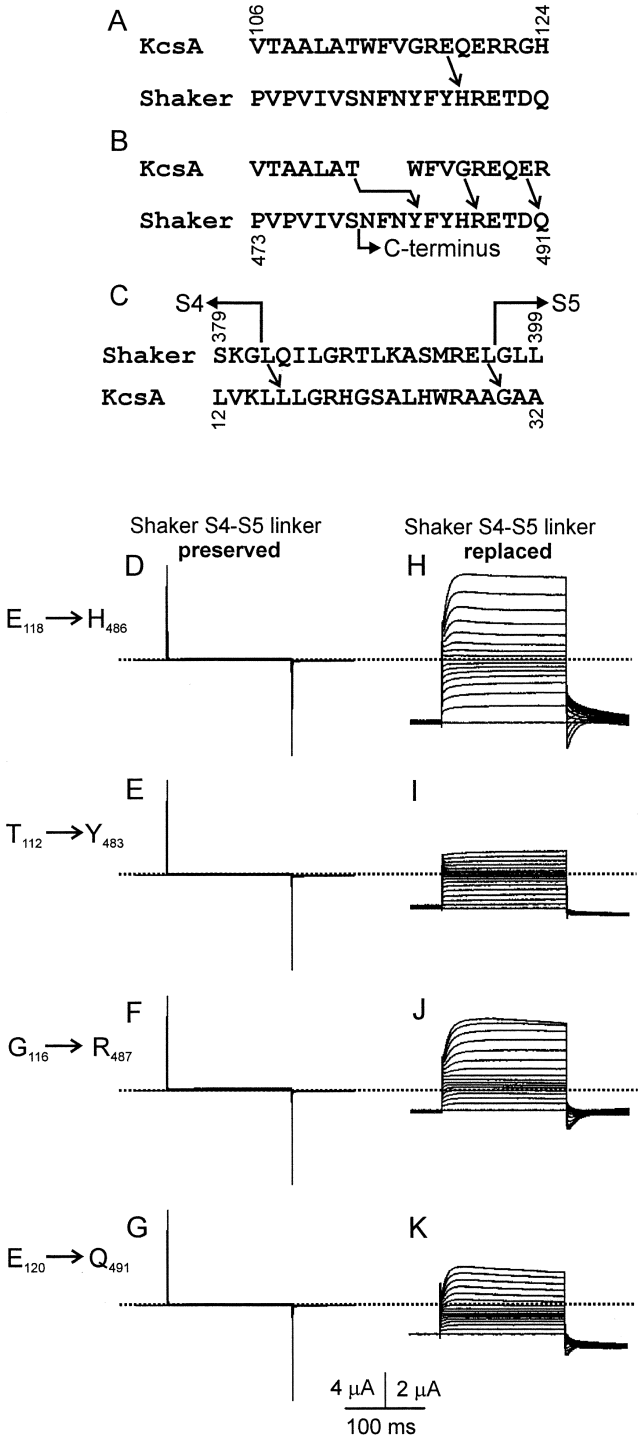

FIGURE 6. Nonfunctional Shaker-KcsA chimeras with various distal COOH-terminal junctions and their rescue by the replacement of the S4–S5 linker. (A and B) Two distinct sequence alignments between Shaker and KcsA in S6/M2-COOH terminus. The distal junction in four chimeric constructs is indicated by the arrows. (C) Alignment of Shaker's S4–S5 linker sequence and its KcsA counterpart (the arrows indicate two alternative proximal junctions). (D–K) Current records from oocytes injected with RNA encoding four chimeras with different distal junctions as indicated. Chimeras corresponding to D-G have a proximal junction that preserves Shaker's S4–S5 linker, whereas in those corresponding to H–K the Shaker S4–S5 linker is replaced by its KcsA counterpart.

T112 and Shaker's Y483 or at two more distal sites (Fig. 6, B and E–G). Remarkably, replacing Shaker's S4–S5 linker by its KcsA counterpart rescues all above four chimeric constructs (Fig. 6 C; D–G versus H–K). Although the mechanism of this rescue phenomenon is unclear, the phenotypes of the rescued constructs are informative in two ways. First, three of the rescued con-

structs exhibit partial voltage sensitivity (Fig. 6, H, J, and K), whereas the fourth construct, whose distal junction connects KcsA's T112 to Shaker's Y483, exhibits practically no voltage dependence (Fig. 6, B and I). The KcsA sequence in the latter chimera is longer than those in most other chimeras in the present study. This observation suggests that the transplanted KcsA pore does not have much intrinsic voltage sensitivity. Second, the chimera with no apparent voltage dependence contains Shaker's COOH-terminal YFYH, whereas the other three chimeras contain KcsA's WFVG (Fig. 6, A and B); in all four the S4–S5 linker is replaced by its KcsA counterpart (Fig. 6 C). Therefore, Shaker's S4–S5 linker and COOH-terminal sequence, or their counterparts in KcsA, apparently work in pair. That is, to be fully gated by voltage a chimeric channel needs to contain both Shaker's S4–S5 linker and its IVSNFNYFY sequence around the gate, with or without the entire preceding PVPV (Figs. 2 C, 3 E, and 5 B). If the pair of sequences are from KcsA, the chimeras exhibit partial voltage sensitivity (Fig. 6, H, J, and K). On the other hand, the chimera is practically not voltage gated when the pair is mismatched, i.e., when Shaker's COOH-terminal YFYH sequence is not paired with its matching S4–S5 linker (Fig. 6 I).

Delineating the Critical Segment in the S4–S5 Linker

To study the S4–S5 linker proper we replaced it with its counterpart from KcsA (Fig. 7 A; B vs. C), or replaced

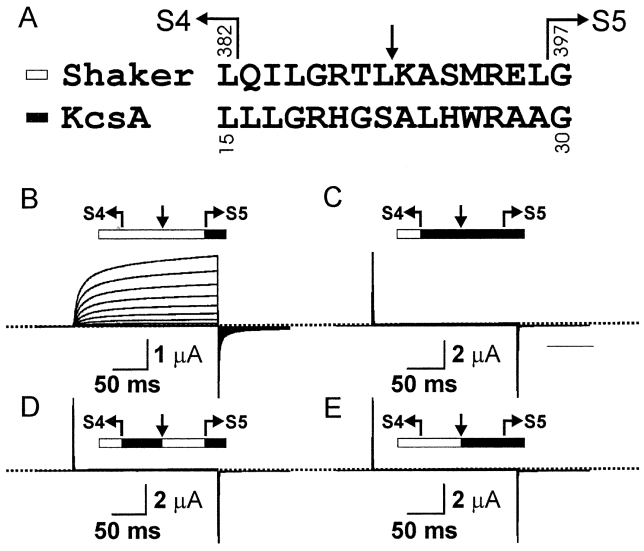

FIGURE 7. Partial and full replacements of the S4–S5 linker by the counterparts in KcsA. All chimeras have an identical distal junction between KcsA's A109 and Shaker's I477 as in Fig. 3 E. (A) Sequence alignment between Shaker's S4–S5 linker and its KcsA counterpart (the downward arrow marks the center of the sequences). (B–E) Current records from chimeras containing Shaker's S4–S5 linker (B), and whose entire linker (C), or the proximal part (D), or the distal part (E) is replaced by the KcsA counterpart as pictured.

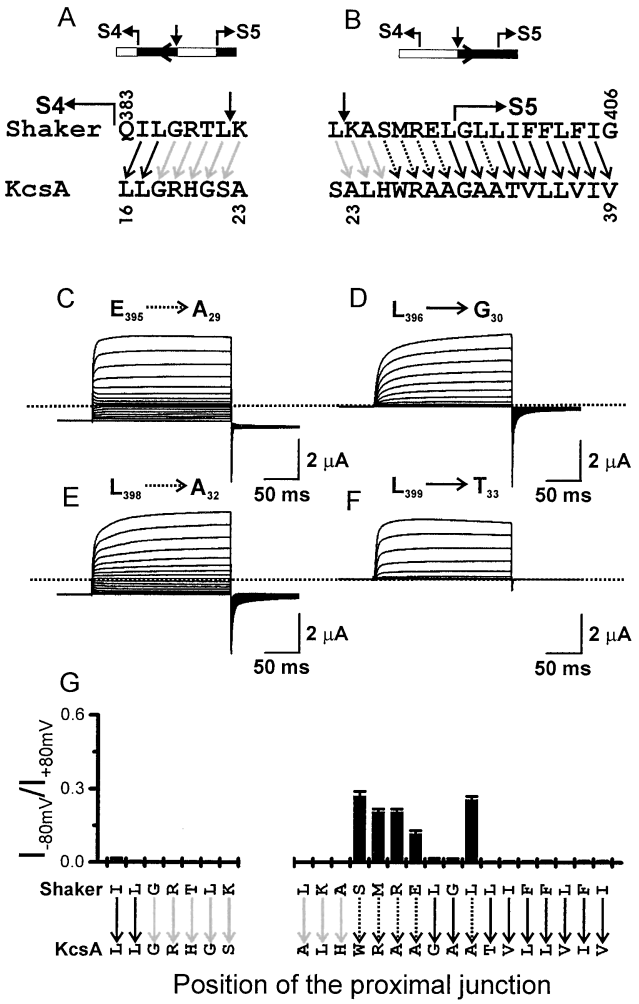

FIGURE 8. Restoration of Shaker's S4–S5 linker sequence. (A and B) Sequence alignment between Shaker's S4–S5 linker through the proximal part of S5 and the KcsA counterpart; the center of the linker is marked by the downward arrows. The arrows in A and B, respectively, indicate a systematic restoration of the Shaker sequence toward S4 and S5 from the center of the S4-S5 linker. The color and type of the arrows represent the chimeras which express minimal (solid black), robust (dotted black) voltage-independent conductance, or electrically nonfunctional chimeric constructs (gray). (C–F) Current records from chimeras with the proximal junction at four different positions. (G) The ratio (mean ± SEM, n = 5–8) of currents at −80 and 80 mV versus the position of the proximal junction in the chimeric constructs.

the proximal and distal portions of the linker separately (Fig. 7, D and E). These replacements were made in a construct with a distal junction between KcsA's A109 and Shaker's I477 as in Fig. 3 E, in which Shaker's S5 through most of S6 is replaced but its COOH terminus is preserved. Each of the three replacements renders the construct expressing no current (Fig. 7, B vs. C–E). To delineate the critical segment we systematically restored the Shaker sequence in the proximal half of the linker, one residue at a time, from the center toward S4 (Fig. 8 A), and separately restored the Shaker

sequence in the distal half of the linker through the initial part of S5 (Fig. 8 B). We found that much of the proximal part of the linker (LGRTLKAS) is essential because it must be restored before the channel becomes functional. Several chimeras with a junction around the distal end of the linker express voltage-independent conductance, whereas those with a junction either further into S5 or near S4 are fully gated (Fig. 8, A, B, and G). Fig. 8, C–F, shows the phenotypes of four chimeric channels whose currents are either partially or fully gated, two of each type, with different proximal junctions. For later reference, we colored part of KcsA's M1 red in the structural model, delineating the region that contains the residues at the varied proximal junction in the chimeric channels expressing voltage-independent conductance at negative voltage (Fig. 11).

In the experiments just described and shown in Fig. 8, we restored Shaker's S4–S5 linker sequence while some residues near the COOH-terminal end of S6 were KcsA's, whereas in those shown in Fig. 3, we replaced the COOH-terminal part of Shaker's S6 with KcsA's M2 while the S4–S5 linker remained Shaker's. In either case, we created mismatches between the sequences in the distal part of the S4–S5 linker (MRELGLL) and the distal part of S6 (PVPVIVS), whose corresponding residues in KcsA are red-colored in the structural model (Fig. 11). A mismatch between these two short sequences caused by mutations (i.e., sequence replacements) results in chimeras expressing voltage-independent conductance at negative voltage.

DRK1-KcsA Chimeras

To test further if the substituting KcsA pore is indeed under the control of the voltage sensors, we made a chimera between KcsA and the DRK1 (K_V 2.1) voltage-gated K^+ channel, because DRK1 is inhibited by HaTx. The toxin inhibits DRK1 by binding to its S3–S4 linker and thereby hindering the movement of its gating charges (Swartz and MacKinnon, 1997a,b; Li-Smerin and Swartz, 2000, 2001; Swartz, 2001). The DRK1-KcsA chimera, depicted in Fig. 9 A, is essentially equivalent to the Shaker-KcsA chimera shown in Fig. 2 A. Like the Shaker-based version, the DRK1-KcsA chimera is voltage gated, conducting minimal if any current at the −80 mV holding potential (Figs. 2 C and 9 C). The midpoint of its G-V curve is significantly shifted, whereas the apparent valence remains essentially unchanged (Fig. 9, B, C, F, and G). The current records of DRK1 and the chimera in the absence and presence of 4 μM HaTx are shown in Fig. 9 (B and C vs. D and E), and the corresponding G-V curves in F and G. Both DRK1 and the chimera are inhibited by gating-modifying HaTx in a comparable manner. These results indicate that the gate in the chimera remains under the control of the voltage sensors.

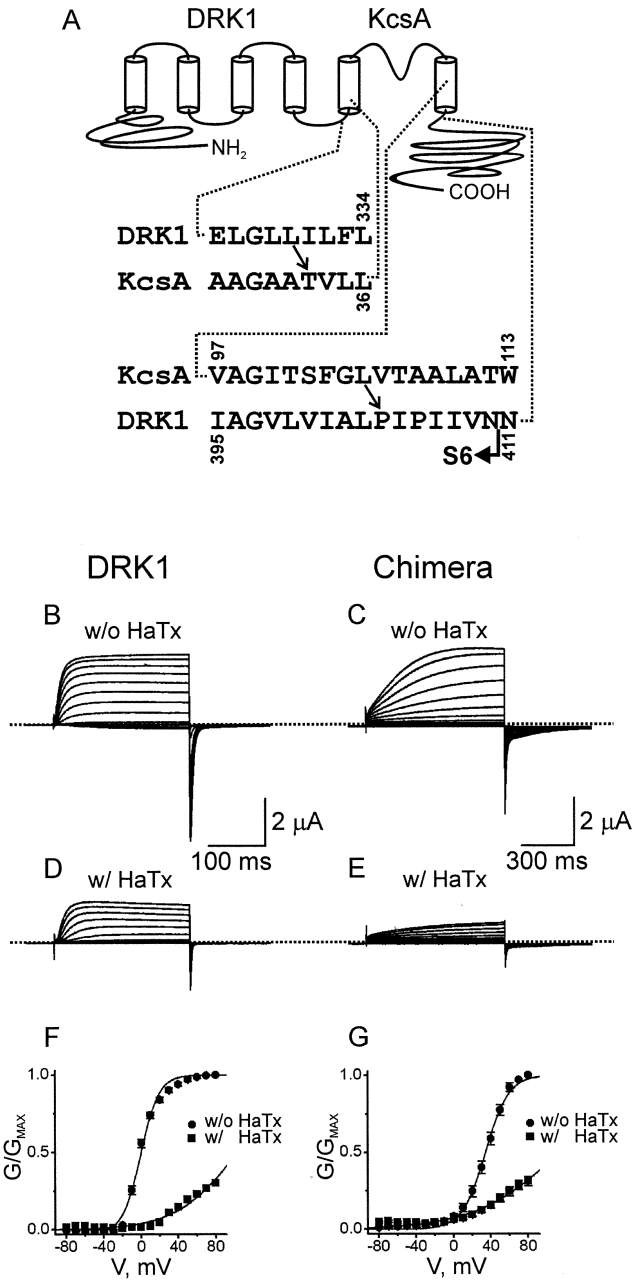

FIGURE 9. A DRK1-KcsA chimera and its HaTx sensitivity. (A) Schema of the polypeptide chain topology of a DRK1-KcsA chimeric channel subunit and partial sequences of the parent channels around the splicing sites. (B–E) Currents of DRK1 (B and D) and the chimera (C and E) without (B and C) and with (D and E) 4 μM HaTx. (F and G) G-V curves for DRK1 and the chimera with and without 4 μM HaTx; the data points represent mean currents (± SEM; n = 6–15). The fitted curves superimposed on the data without HaTx correspond to the Boltzmann function, yielding $V_{1/2} = -0.4 \pm 1.0$ mV and $Z = 2.5 \pm 0.3$ for DRK1, and $V_{1/2} = 35.1 \pm 0.4$ mV and $Z = 2.2 \pm 0.4$ for the chimera. The curves on the data with HaTx have no physical meaning.

As in the case of Shaker, a further extension of the replacing KcsA sequence in either the proximal or the distal direction results in voltage-independent conduc-

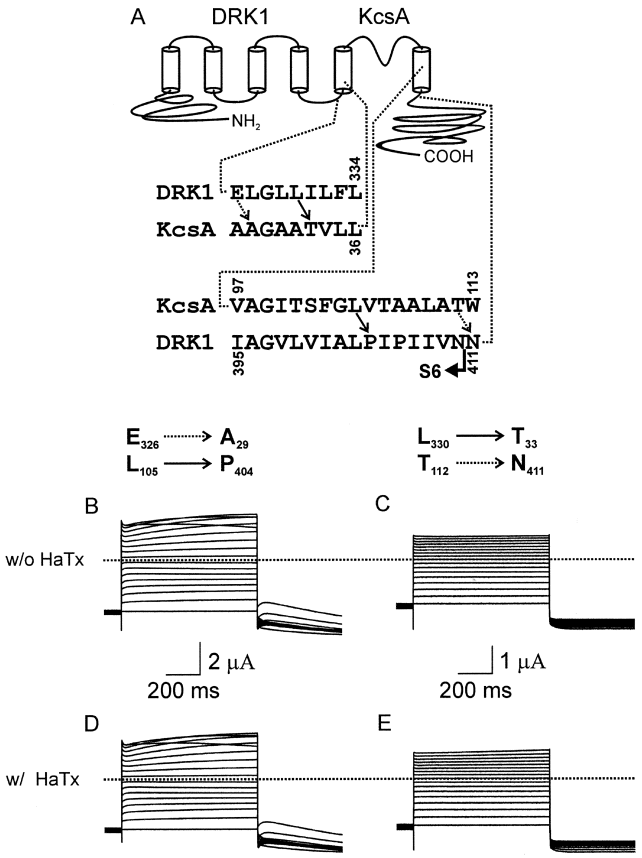

FIGURE 10. Effects of including more KcsA pore residues by moving the junctions in the DRK1-KcsA chimera proximally or distally. (A) Schema of the polypeptide chain topology of a DRK1-KcsA chimeric channel subunit and partial sequences of the parent channels around the splicing sites. The shown chimera corresponding to B and D has the same distal junction as that in Fig. 9, A and C, but a different proximal junction (solid versus dotted arrow), whereas the one corresponding to C and E has the same proximal junction as that in Fig. 9, A and C, but a different distal junction (solid vs. dotted arrows). Currents shown were recorded in either the absence (B and C) or the presence (D and E) of 4 μM HaTx.

tance at negative voltage. For example, moving the proximal junction from between DRK1's L330 and KcsA's T33 (solid arrow in Fig. 10 A) to between E326 and A29 (dotted arrow) results in a chimera that exhibits little depolarization-activating current (Fig. 10 B). The decrease in current at very positive voltages is most probably due to channel inactivation and/or block, which recovers slowly upon hyperpolarization. Also, as shown in Fig. 10 C, moving the distal junction from between KcsA's L105 and DRK1's P404 (solid arrow) to between T112 and N411 (dotted arrow) results in a chimera that exhibits practically no depolarization-activating current, even though it contains a longer KcsA sequence than the fully gated one shown in Fig. 9 C. These findings are also consistent with the scenario that the transplanted KcsA pore does not have much intrinsic voltage sensitivity. Furthermore, the two chimeric channels exhibiting little or no depolarization-activated current are not inhibited by 4 μM HaTx (Fig. 10, B vs. D, C vs. E). Thus, the channel gate in these HaTx-insensitive chimeras may no longer be controlled by the voltage sensors.

DISCUSSION

Shaker and DRK1 remain voltage gated even when their S5 through most of S6 is replaced by its counterpart in KcsA (Figs. 2 C and 9 C), which is represented by the blue ribbon shown in Fig. 11. The G-V curves of the chimeras have valences comparable to those of the corresponding parent voltage-gated channels (Figs. 2 D, and 9, F vs. G). Like the wild-type, the DRK1 mutant is also inhibited by HaTx (Fig. 9, B–G). Since HaTx inhibits DRK1 by hindering the movement of gating charges, the HaTx sensitivity of the chimera indicates that its gate remains under control of the voltage sensors (Swartz and MacKinnon, 1997a,b; Li-Smerin and Swartz, 2000, 2001; Swartz, 2001). Consequently, as shown in Fig. 5 C, the time course of the chimeric channel activation remains sigmoidal. In contrast, Shaker and DRK1 with longer substituting KcsA sequences exhibit partial-or-no activation-and-deactivation upon changing membrane voltage (Figs. 3, 6, 8, and 10). The DRK1-based chimeras exhibiting little or no voltage activation are HaTx insensitive (Fig. 10). Together, the correlation between the voltage dependency and HaTx sensitivity in the chimeras, and the fact that increasing the length of the replacing KcsA pore sequence reduces the voltage dependence of the chimeras, are highly consistent with the scenario that the observed voltage dependence primarily reflects the property of voltage-sensing modules in Shaker or DRK1, not the substituting KcsA pore sequence. This is further supported by the observation that an inward rectifier whose pore is replaced by KcsA's still acts as an inward rectifier, not a voltage-gated channel, displaying no depolarization-induced activation (Lu et al., 2001).

To obtain a channel fully gated by voltage, Shaker's S4–S5 linker (LGRTLKASMRELGLL) and the sequence around the COOH-terminal end of S6 (PVPVIVSNFNYFY) must be preserved. A mismatch between the distal portion of the former (MRELGLL) and proximal portion of the latter (PVPVIVS) caused by replacing either of them, partially or entirely, results in voltage-independent conductance (Figs. 3 and 8). The distal part of the S4–S5 linker in Shaker (MRELGLL) actually corresponds to the proximal portion of M1 in KcsA (WRAAGAA) because M1 in KcsA is longer than the traditionally defined S5 in Shaker. To gain insight into the spatial relation of the Shaker sequence pair, we colored their KcsA counterparts red in the structural model (Fig. 11), showing the two sequences

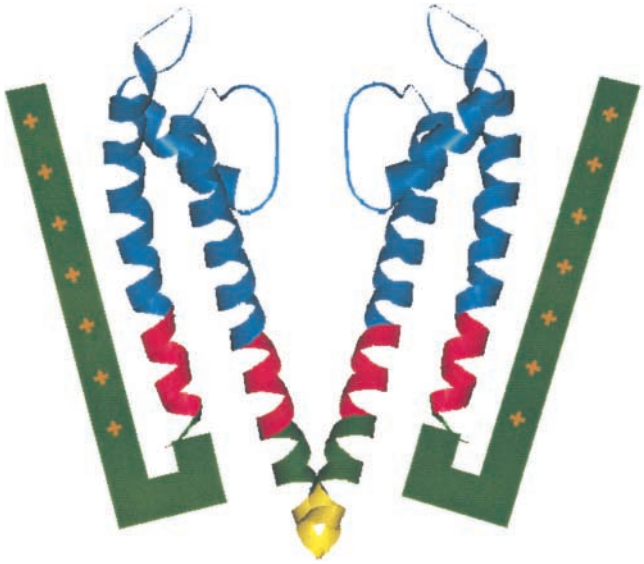

FIGURE 11. A cartoon of two Shaker subunits in the region from S4 to the initial part of the COOH terminus. Each ribbon corresponds to the structure of a KcsA subunit (Zhou et al., 2001). In each subunit, the blue region corresponds to T33 in M1 through L105 in M2, the red regions to W26-A32 in M1 and V106-T112 in M2, the green region to W113-E118 in M2, and the yellow region to Q119–A124. Each green strip represents S4 through the proximal part of the "S4–S5 linker."

located side by side and packed together. Each green strip in the model represents S4 through the remaining, proximal part of the S4–S5 linker. The proximal part of the S4–S5 linker (LGRTLKAS) and the beginning of Shaker's COOH terminus (NFNYFY) also work in pair. The latter corresponds to the distal portion of M2 in KcsA (green-colored ribbon in Fig. 11) because the traditionally defined S6 is shorter than M2 in KcsA. To be fully gated by voltage a channel needs to contain both of these Shaker sequences (Fig. 2). If the pair of sequences are from KcsA the chimeras are partially voltage sensitive (Fig. 6, H, J, and K). On the other hand, the chimera is not gated by voltage when the pair is mismatched, that is, when Shaker's COOH-terminal sequence is not paired with its matching sequence in the S4–S5 linker (Fig. 6 I). Therefore, the complementary Shaker sequences, LGRTLKASMRELGLL and PVPVIVSNFNYFY, work in pair. Multiple interactions between the two sequences help to explain why Shaker's gating is profoundly affected here by multiple mutations (i.e., sequence replacements), but only modestly affected by most single-point mutations in some previous studies (e.g., Holmgren et al., 1996; Li-Smerin et al., 2000), with the exception of a drastic mutation, P475D, which also causes voltage-independent conductance (Hackos et al., 2002).

The voltage-independent conductance may reflect loosened coupling between the voltage sensors and the channel gate. Since sequential models are usually used to describe voltage sensing and gating in K^+ channels, we will first consider the voltage-independent conductance in the frame of a sequential, obligatory model and then an allosteric model. The commonly used sequential kinetic models contain at least five closed states and one open state, in which four voltage sensors move independently while the final concerted step leads to opening of the pore (Fig. 12 A; Hodgkin and Huxley, 1952; Bezanilla et al., 1994; Zagotta et al., 1994; Schoppa and Sigworth, 1998; Horn et al., 2000). The model implies that the channel gate is unable to open without the preceding movement of the voltage sensors. For simplicity, in the steady state the sequential model with multiple steps for voltage sensing and gating may be approximated by a model with a single step (Fig. 12 B). In the latter, the channel gate is closed (C_{S4}) when the voltage-sensing S4 is in the resting state, whereas it opens (O^{S4}) when the sensors become activated by depolarization. Any voltage-independent opening reflects that of a channel whose gate is decoupled from the sensors so that it is no longer under their control, as represented by state "O" (Fig. 12 C). According to the model, the G-V curve is given by:

$$\frac{G}{G_{MAX}} = \frac{1}{1 + \dfrac{1}{K_C + K_{SG} e^{\frac{ZFV_m}{RT}}}}, \qquad (1)$$

where K_C is the equilibrium constant for the coupling step between the voltage sensors and the gate, defined as the ratio of [O] and [C_{S4}] and assumed to be voltage independent. K_{SG} is the overall equilibrium constant for the voltage sensing and gating process, defined as the ratio of [O^{S4}] and [C_{S4}]. Quantities Z, F, V_m, R, and T have their usual meaning. If the gate is fully coupled to the voltage sensors, K_C is zero and Eq. 1 becomes:

$$\frac{G}{G_{MAX}} = \frac{1}{1 + \dfrac{1}{K_{SG} e^{\frac{ZFV_m}{RT}}}}, \qquad (2)$$

which is the Boltzmann function. However, if the coupling were sufficiently disrupted by mutations, K_C would then be nonzero. Consequently, at negative voltage Eq. 1 approaches the minimum:

$$\frac{G_{MIN}}{G_{MAX}} = \frac{1}{1 + \dfrac{1}{K_C}}, \qquad (3)$$

producing voltage-independent conductance at negative voltage, whose magnitude is determined by K_C. Therefore, the voltage-independent conductance observed with some chimeras can be accounted for by loosened coupling between the voltage sensors and the channel gate.

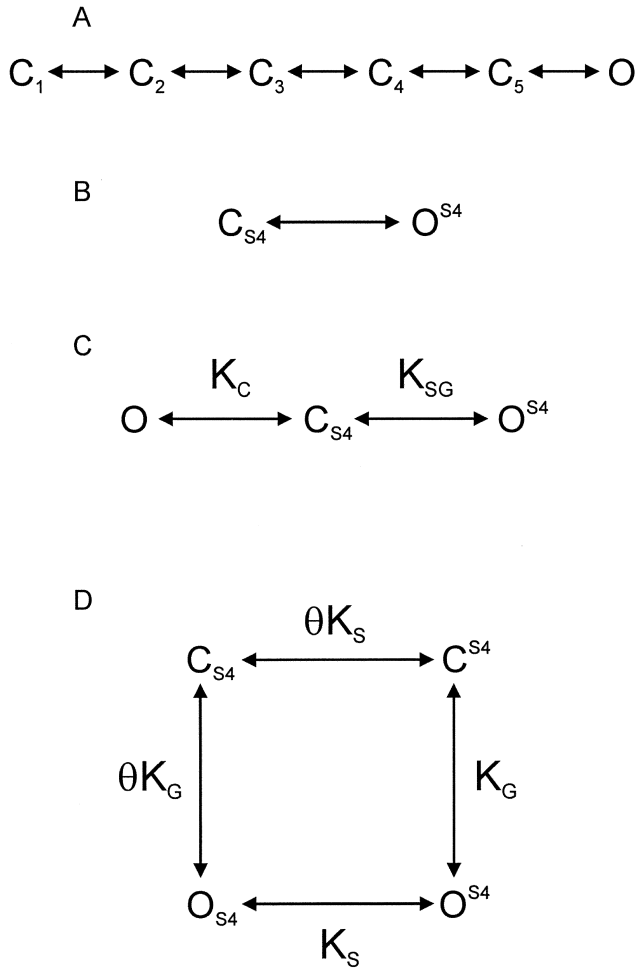

FIGURE 12. Minimal gating models. (A) A sequential model containing five closed states "C" and an open state "O". (B) A minimal model reduced from that shown in A, where the channel is closed when the S4 is in the resting state (C_{S4}), or open when the S4 is activated upon depolarization (O^{S4}). (C) The minimal model shown in B with an additional transition accounting for the coupling interaction between the voltage sensors and the channel gate. It contains one closed state where the gate is coupled to the voltage sensors in the resting state (C_{S4}), and two open states where the gate is coupled to the voltage sensors in the activated state (O^{S4}) or it is decoupled from the sensors (O). K_C is the equilibrium constant for the coupling step between the sensors and the gate, and K_{SG} for the overall voltage sensing and gating transition. (D) A four-state allosteric model, where the voltage sensors move in the horizontal transitions, whereas the gate moves in the vertical. The gate can open with or without activating the voltage sensors (O^{S4} or O_{S4}). K_S and K_G are, respectively, the equilibrium constants for the lower horizontal and the right vertical transitions. The coupling constant Θ is defined as the ratio of the equilibrium constants either for the gating transitions without and with activating the voltage sensors, or for the voltage-sensing transitions without and with opening of the gate.

We consider next the observed voltage-independent conductance in the frame of an allosteric model (Monod et al., 1965). Fig. 12 D shows a four-state allosteric model which assumes that the gate can open spontaneously even without activating the voltage sensors (C_{S4} to O_{S4}). In the model, voltage sensors move in the horizontal transitions while the gate moves in the vertical. K_S is the equilibrium constant for the lower horizontal transition, and K_G for the right vertical transition which is assumed to be voltage independent. The coupling constant, Θ, is defined as the ratio of the equilibrium constants either for the gating transitions without and with activating the voltage sensors, or for the voltage-sensing transitions without and with opening of the gate. Constant Θ becomes smaller as the coupling strength increases. The G-V curve of the model is given by:

$$\frac{G}{G_{MAX}} = \frac{1}{1 + \dfrac{1 + \theta K_s e^{\frac{ZFV}{RF}}}{\left(1 + K_s e^{\frac{ZFV}{RF}}\right)\theta K_G}}. \qquad (4)$$

Fig. 13 A shows a series of simulated G-V curves with different coupling strength using Eq. 4, where for simplicity, $K_S = 10^{-9}$, $K_G = 1$, and $Z = 12$ (Schoppa et al., 1992), whereas Θ is varied from 10^{-9} to 1 in 10-fold increments (Islas and Sigworth, 1999). As the coupling is loosened by increasing Θ, the voltage-independent conductance increases and the channel eventually loses its voltage dependence completely. Thus, in the allosteric model the voltage-independent conductance can also be accounted for by loosened coupling. Fig. 13 B shows another series of simulated G-V curves with the gating transition in different equilibria, where $K_S = 10^{-9}$, $\Theta = 10^{-9}$, and $Z = 12$, whereas K_G is varied from 1 to 10^{13} in 10-fold increments. With a shift of the gating equilibrium toward the open state by increasing K_G, the voltage-independent conductance increases and the channel eventually loses its voltage dependence too. The above exercises show that the voltage-independent conductance can in theory be accounted for by not only loosened coupling, but also a dramatic increase in the gating equilibrium constant (K_G) by the order of 10^9–10^{13} (ΔG = 12–18 kcal/mole), provided that the gate is not under obligatory, but allosteric, control of the voltage sensors.

Allosteric models have been used to describe complex gating in a number of ion channels that exhibit spontaneous openings. For example, acetylcholine receptor channels and cyclic nucleotide–gated channels exhibit unliganded openings (Jackson, 1984, 1988; Ruiz and Karpen, 1997; Tibbs et al., 1997). The mSlo K^+ channel, activated by Ca^{2+} and voltage, also appears to open spontaneously because in a nominal absence of Ca^{2+}, the open probability of mSlo does not further decrease steeply with hyperpolarization when it reaches the range of 10^{-6}–10^{-5} (Cox et al., 1997; Horrigan et al., 1999; Horrigan and Aldrich, 1999). However, in the

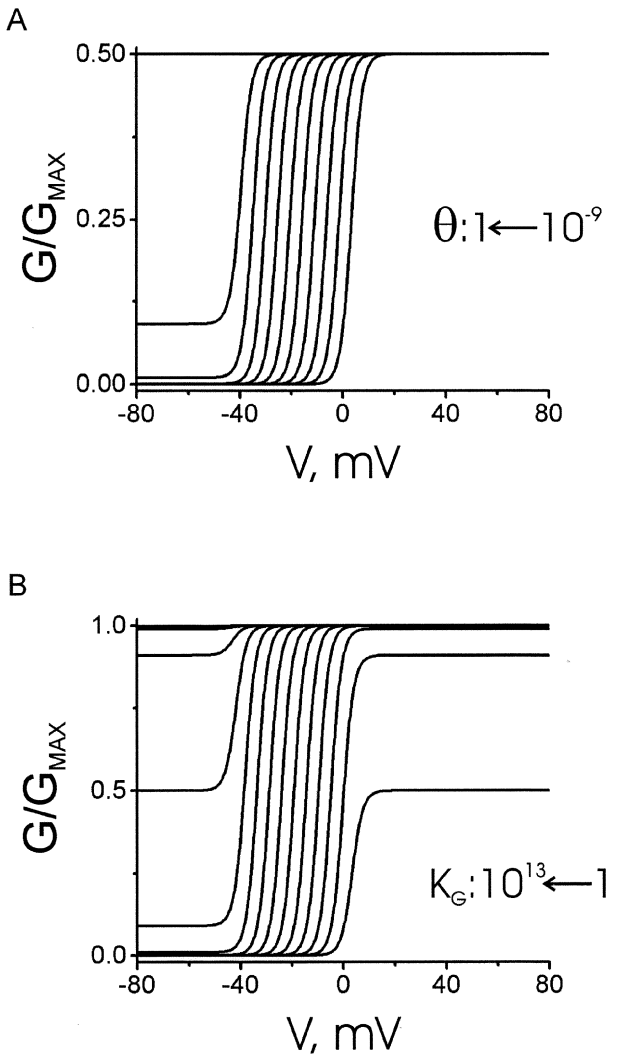

FIGURE 13. Simulations of G-V curves. (A) Simulated G-V curves with different coupling strength using equation 4, where $K_S = 10^{-9}$, $K_G = 1$, and $Z = 12$, whereas Θ is varied from 10^{-9} to 1 (right to left) in 10-fold increments. (B) Simulated G-V curves with the gating transition in different equilibria, where $K_S = 10^{-9}$, $\Theta = 10^{-9}$, and $Z = 12$, whereas K_G is varied from 1 to 10^{13} (right to left) in 10-fold increments.

case of Shaker and DRK1 voltage-gated K^+ channels, the steepness of the semilogarithmic P_O-V plots remains undiminished even as its open probability is reduced to as low as $\sim 10^{-7}$ at negative voltage, and no voltage-independent opening was observed (Islas and Sigworth, 1999). Based on these and other findings, the authors argue that the voltage sensors are coupled to the gate in Shaker and DRK1 channels via an obligatory rather than a traditional allosteric mechanism (compare Zagotta et al., 1994; Horrigan et al., 1999). In principle, the two mechanisms require different structural properties. Recent crystallographic studies show that in a bacterial Ca^{2+}-gated K^+ channel with only two transmembrane segments per subunit, the Ca^{2+} sensors formed by part of the COOH terminus are directly connected to the gate in the last transmembrane segment (Jiang et al., 2002a,b). However, in the case of Shaker, the kinetic energy in the voltage-sensing S4 is undoubtedly not transmitted to the gate in S6 via the connecting main peptide chain that forms the K^+-selectivity filter. Instead, it is most probably via some interfaces among the involved elements (Li-Smerin et al., 2000; Lu et al., 2001; for review see Horn, 2000). In the case of an obligatory mechanism, the coupling interfaces must be tight with practically no compliance unless there is a permissible toggle switch, whereas an appropriate amount of compliance would be expected for an allosteric mechanism.

As a third possibility, voltage-independent conductance at negative voltage could occur if mutations had destroyed the intracellular gate, whereas the observed partial voltage sensitivity might reflect additional, incomplete gating by the K^+ selectivity filter (Chapman et al., 1997; Zheng and Sigworth, 1997). It predicts that hyperpolarization would reduce the open channel probability to the same value for all chimeric channels whose intracellular gate had been destroyed. Contrary to this, the plateau amplitude of the G-V curve (reflecting the open probability) at negative voltage actually varies greatly among the different chimeric channels (Fig. 3 F). Furthermore, at negative voltage a chimeric channel that expresses voltage-independent conductance does enter the closed state and exhibit a lower open probability (Fig. 4). These findings indicate that the intracellular activation gate is neither significantly leaky nor totally destroyed.

In summary, the complementarity of a pair of Shaker sequences, located internal to the hypothesized gating hinge (Jiang et al., 2002b), is essential for the channel to reduce its open probability to the minimum in response to membrane hyperpolarization. One sequence is the so called S4–S5 linker (LGRTLKASMRELGLL) distal to the voltage-sensing S4, while the other is around the COOH-terminal end of S6 (PVPVIVSNFNYFY), a region containing the actual gate-forming residues (Liu et al., 1997; Hackos et al., 2002). The KcsA counterparts for the more external portion of the Shaker sequence pair are packed together in the crystal structure (red-colored in Fig. 11). A disruption of the complementarity between the two sequences from Shaker (or DRK1) by mutations causes voltage-independent conductance at negative voltage or even a complete loss of voltage dependence. Although not exclusively, the voltage-independent conductance resulting from mutating either of the two sequences can be fully accounted for by loosened coupling between the voltage sensors and the activation gate, with or without a concurrent shift of the gating equilibrium. The scenario of loosened coupling becomes even more likely if

the coupling mechanism between the voltage sensors and the activation gate is obligatory rather than allosteric. On the basis of all the above, we propose that the complementary Shaker sequence pair, LGRTLKASMRELGLL and PVPVIVSNFNYFY, form a critical part of the structure that allows the voltage sensors to control the intracellular activation gate. Figuratively, if the COOH-terminal part of S6 and its immediate extension are viewed as the "door handle" (Lu et al., 2001), the S4–S5 linker would be the "hand." One may then imagine that as the "arm" (S4) descends and/or rotates upon membrane hyperpolarization, the hand pushes the door handle to close the gate. If such an action from one arm leads to a closure of the gate, all four must be brought back before the gate can open. This scheme is compatible with the usual minimal kinetic model for voltage gating, which contains four independent voltage-sensing transitions that precedes a concerted step leading to opening of the pore (Hodgkin and Huxley, 1952; Bezanilla et al., 1994; Zagotta et al., 1994; Schoppa and Sigworth, 1998; Horn et al., 2000).

We thank P. De Weer, F.T. Horrigan, and K.J. Swartz for critical review and discussions of our manuscript, and many other colleagues for helpful discussions, R. MacKinnon for DRK1 and KcsA cDNAs, and K.J. Swartz for Shaker-IR cDNA subcloned in the pGEM-HESS vector.

This study was supported by National Institutes of Health grants GM55560 and GM61929. Z. Lu is a recipient of an Independent Scientist Award from National Institutes of Health (HL03814).

Submitted: 9 August 2002
Revised: 24 September 2002
Accepted: 25 September 2002

REFERENCES

Aggarwal, S.K. 1996. Analysis of the voltage-sensor in a voltage-activated potassium channel. Ph.D. thesis. Harvard University, Cambridge, MA.

Aggarwal, S.K., and R. MacKinnon. 1996. Contribution of the S4 segment to gating charge in the Shaker K^+ channel. *Neuron.* 16: 1169–1177.

Armstrong, C.M. 1971. Interaction of tetraethylammonium ion derivatives with the potassium channels of giant axons. *J. Gen. Physiol.* 58:413–437.

Bezanilla, F., E. Perozo, and E. Stefani. 1994. Gating of Shaker K^+ channels: II. The components of gating currents and a model of channel activation. *Biophys. J.* 66:1011–1021.

Caprini, M., S. Ferroni, R. Planells-Cases, J. Rueda, C. Rapisarda, A. Ferrer-Montiel, and M. Montal. 2001. Structural compatibility between the putative voltage sensor of voltage-gated K^+ channels and the prokaryotic KcsA channel. *J. Biol. Chem.* 276:21070–21076.

Cha, A., G.E. Snyder, P.R. Selvin, and F. Bezanilla. 1999. Atomic scale movement of the voltage-sensing region in a potassium channel measured via spectroscopy. *Nature.* 402:809–813.

Chapman, M.L., H.M. VanDongen, and A.M. VanDongen. 1997. Activation-dependent subconductance levels in the drk1 K^+ channel suggest a subunit basis for ion permeation and gating. *Biophys. J.* 72:708–719.

Cortes, D.M., and E. Perozo. 1997. Structural dynamics of the *Streptomyces lividans* K^+ channel (SKC1): oligomeric stoichiometry and stability. *Biochemistry.* 36:10343–10352.

Cox, D.H., J. Cui, and R.W. Aldrich. 1997. Allosteric gating of large conductance Ca-activated K^+ channel. *J. Gen. Physiol.* 110:257–281.

del Camino, D., M. Holmgren, Y. Liu, and G. Yellen. 2000. Blocker protection in the pore of a voltage-gated K^+ channel and its structural implications. *Nature.* 403:321–325.

del Camino, D., and G. Yellen. 2001. Tight steric closure at the intracellular activation gate of a voltage-gated K^+ channel. *Neuron.* 32:649–656.

Doyle, D.A., C.J. Morais, R.A. Pfuetzner, A. Kuo, J.M. Gulbis, S.L. Cohen, B.T. Chait, and R. MacKinnon. 1998. The structure of the potassium channel: molecular basis of K^+ conduction and selectivity. *Science.* 280:69–77.

Frech, G.C., A.M. VanDongen, G. Schuster, A.M. Brown, and R.H. Joho. 1989. A novel potassium channel with delayed rectifier properties isolated from rat brain by expression cloning. *Nature.* 340:642–645.

Garcia, M.L., M. Garcia-Calvo, P. Hidalgo, A. Lee, and R. MacKinnon. 1994. Purification and characterization of three inhibitors of voltage-dependent K^+ channels from *Leiurus quinquestriatus* var. *hebraeus* venom. *Biochemistry.* 33:6834–6839.

Glauner, K.S., L.M. Mannuzzu, C.S. Gandhi, and E.Y. Isacoff. 1999. Spectroscopic mapping of voltage sensor movement in the Shaker potassium channel. *Nature.* 402:813–817.

Hackos, D.A., T.-H. Chang, and K.J. Swartz. 2002. Scanning the intracellular S6 activation gate in the Shaker K^+ channel. *J. Gen. Physiol.* 119:521–532.

Hackos, D.H., and K.J. Swartz. 2001. Disrupting the cytoplasmic gate in the Shaker K^+ channel with mutations in S6. *Biophys. J.* 80:182a–183a.

Heginbotham, L., E. Odessey, and C. Miller. 1997. Tetramer stoichiometry of a prokaryotic K^+ channel. *Biochemistry.* 36:1613–1619.

Ho, K., C.G. Nichols, W.J. Lederer, J. Lytton, P.M. Vassilev, M.V. Kanazirska, and S.C. Hebert. 1993. Cloning and expression of an inwardly rectifying ATP-regulated potassium channel. *Nature.* 362:31–38.

Hodgkin, A.L., and A.F. Huxley. 1952. A quantitative description of membrane current and its application to conduction and excitation in muscle. *J. Physiol.* 117:500–544.

Holmgren, M., M.E. Jurman, and G. Yellen. 1996. N-type inactivation and the S4-S5 region of the Shaker K^+ channel. *J. Gen. Physiol.* 108:195–206.

Holmgren, M., K.S. Shin, and G. Yellen. 1998. The activation gate of a voltage-gated K^+ channel can be trapped in the open state by an intersubunit metal bridge. *Neuron.* 21:617–621.

Holmgren, M., P.L. Smith, and G. Yellen. 1997. Trapping of organic blockers by closing of voltage-dependent K^+ channels: evidence for a trap door mechanism of activation gating. *J. Gen. Physiol.* 109:527–535.

Horn, R. 2000. Conversation between voltage sensors and gates of ion channels. *Biochemistry.* 39:15653–15658.

Horn, R., S. Ding, and H.J. Gruber. 2000. Immobilizing the moving parts of voltage-gated ion channels. *J. Gen. Physiol.* 116:461–475.

Horrigan, F.T., J. Cui, and R.W. Aldrich. 1999. Allosteric voltage gating of potassium channels I: mSlo ionic currents in the absence of Ca^{2+}. *J. Gen. Physiol.* 114:277–304.

Horrigan, F.T., and R.W. Aldrich. 1999. Allosteric voltage gating of potassium channels II: mSlo channel gating charge movement in the absence of Ca^{2+}. *J. Gen. Physiol.* 114:305–336.

Hoshi, T., W.N. Zagotta, and R.W. Aldrich. 1990. Biophysical and molecular mechanisms of *Shaker* potassium channel inactivation. *Science.* 250:533–538.

Hoshi, T., W.N. Zagotta, and R.W. Aldrich. 1991. Two types of inac-

tivation in Shaker K^+ channels: effects of alterations in the carboxy-terminal region. *Neuron.* 7:547–556.

Islas, L.D., and F.J. Sigworth. 1999. Voltage sensitivity and gating charge in Shaker and Shab family potassium channels. *J. Gen. Physiol.* 114:723–741.

Jackson, M.B. 1984. Spontaneous openings of the acetylcholine receptor channel. *Proc. Natl. Acad. Sci. USA.* 81:3901–3904.

Jackson, M.B. 1988. Dependence of acetylcholine receptor channel kinetics on agonist concentration on culture muscle fibers. *J. Physiol.* 397:555–583.

Jiang, Y., A. Lee, J. Chen, M. Cadene, B.T. Chait, and R. MacKinnon. 2002a. Crystal structure and mechanism of a calcium-gated potassium channel. *Nature.* 417:515–522.

Jiang, Y., A. Lee, J. Chen, M. Cadene, B.T. Chait, and R. MacKinnon. 2002b. The open pore conformation of potassium channels. *Nature.* 417:523–526.

Kamb, A., J. Tseng-Crank, and M.A. Tanouye. 1988. Multiple products of the *Drosophila* Shaker gene may contribute to potassium channel diversity. *Neuron.* 1:421–430.

Kubo, Y., T.J. Baldwin, Y.N. Jan, and L.Y. Jan. 1993. Primary structure and functional expression of a mouse inward rectifier potassium channel. *Nature.* 362:127–133.

Larsson, H.P., O.S. Baker, D.S. Dhillon, and E.Y. Isacoff. 1996. Transmembrane movement of the Shaker K^+ channel S4. *Neuron.* 16:387–397.

Li-Smerin, Y., D.H. Hackos, and K.J. Swartz. 2000. A localized interaction surface for voltage-sensing domains on the pore domain of a K^+ channel. *Neuron.* 25:411–423.

Li-Smerin, Y., and K.J. Swartz. 1998. Gating modifier toxins reveal a conserved structural motif in voltage-gated Ca^{2+} and K^+ channels. *Proc. Natl. Acad. Sci. USA.* 95:8585–8589.

Li-Smerin, Y., and K.J. Swartz. 2000. Localization and molecular determinants of the hanatoxin receptors on the voltage-sensing domains of a K^+ channel. *J. Gen. Physiol.* 115:673–684.

Li-Smerin, Y., and K.J. Swartz. 2001. Helical stucture of the COOH terminus of S3 and its contribution to the gating modifier toxin receptor in voltage-gated ion channels. *J. Gen. Physiol.* 117:205–217.

Liman, E.R., P. Hess, F. Weaver, and G. Korean. 1991. Voltage-sensing residues in the S4 region of a mammalian K^+ channel. *Nature.* 353:752–756.

Liu, Y., M. Holmgren, M.E. Jurman, and G. Yellen. 1997. Gated access to the pore of a voltage-dependent K^+ channel. *Neuron.* 19: 175–184.

Lu, Z., A.M. Klem, and Y. Ramu. 2001. Ion conduction pore is conserved among potassium channels. *Nature.* 413:809–813.

MacKinnon, R. 1991. Determination of the subunit stoichiometry of a voltage-activated potassium channel. *Nature.* 350:232–235.

MacKinnon, R., S.L. Cohen, A. Kuo, A. Lee, and B.T. Chait. 1998. Structural conservation in prokaryotic and eukaryotic potassium channels. *Science.* 280:106–109.

Mannuzzu, L.M., M.M. Moronne, and E.Y. Isacoff. 1996. Direct physical measure of conformational rearrangement underlying potassium channel gating. *Science.* 271:213–216.

Monod, J., J. Wyman, and J.-P. Changeux. 1965. On the nature of allosteric transitions: a plausible model. *J. Mol. Biol.* 12:88–118.

Morais-Cabral, J.H., Y. Zhou, and R. MacKinnon. 2001. Energetic optimization of ion conduction rate by the K^+ selectivity filter. *Nature.* 414:37–42.

Papazian, D.M., L.C. Timpe, Y.N. Jan, and L.Y. Jan. 1991. Alteration of voltage-dependence of Shaker potassium channel by mutations in the S4 sequence. *Nature.* 349:305–310.

Perozo, E., D.M. Cortes, and L.G. Cuello. 1999. Structural rearrangements underlying K^+-channel activation gating. *Science.* 285:73–78.

Perozo, E., L. Santacruz-Toloza, E. Stefani, F. Benzanilla, and D.M. Papazian. 1994. S4 mutations alter gating currents of Shaker K^+ channels. *Biophys. J.* 66:345–354.

Pongs, O., N. Kecskemethy, R. Muller, I. Krah-Jentgens, A. Baumann, H.H. Kiltz, I. Canal, S. Llamazares, and A. Ferrus. 1988. Shaker encodes a family of putative potassium channel proteins in the nervous system of *Drosophila. EMBO J.* 7:1087–1096.

Ruiz, M.L., and J.W. Karpen. 1997. Single cyclic nucleotide-gated channels locked in different ligand-bound states. *Nature.* 389: 389–392.

Schoppa, N.E., K. McCormack, M.A. Tanouye, and F.J. Sigworth. 1992. The size of gating charge in wild-type and mutant *Shaker* potassium channels. *Science.* 255:1712–1715.

Schoppa, N.E., and F.J. Sigworth. 1998. Activation of Shaker potassium channels. III: An activation gating model for wild-type and V2 mutant channels. *J. Gen. Physiol.* 111:313–342.

Schrempf, H., O. Schmidt, R. Kummerlen, S. Hinnah, D. Muller, M. Betzler, T. Steinkamp, and R. Wagner. 1995. A prokaryotic potassium ion channel with two predicted transmembrane segments from *Streptomyces lividans. EMBO J.* 14:5170–5178.

Seoh, S.-A., D. Sigg, D.M. Papazian, and F. Bezanilla. 1996. Voltage-sensing residues in the S2 and S4 segments of the Shaker K^+ channel. *Neuron.* 16:1159–1167.

Swartz, K.J. 2001. Independent movement of voltage-sensing domains in the DRK1 K^+ channel revealed by a gating modifier toxin. *Biophys. J.* 80:440a.

Swartz, K.J., and R. MacKinnon. 1995. An inhibitor of the Kv2.1 potassium channel isolated from the venom of a Chilean tarantula. *Neuron.* 15:941–949.

Swartz, K.J., and R. MacKinnon. 1997a. Hanatoxin modifies the gating of a voltage-dependent K^+ channel through multiple binding sites. *Neuron.* 18:665–673.

Swartz, K.J., and R. MacKinnon. 1997b. Mapping the receptor site for hanatoxin, a gating modifier of voltage-dependent K^+ channels. *Neuron.* 18:675–682.

Tempel, B.L., D.M. Papazian, T.L. Schwarz, Y.N. Jan, and L.Y. Jan. 1987. Sequence of a probable potassium channel component encoded at Shaker locus of *Drosophila. Science.* 237:770–775.

Tibbs, G.R., E.H. Goulding, and S.A. Siegelbaum. 1997. Allosteric activation of and tuning of ligand efficacy in cyclic-nucleotide gated channels. *Nature.* 386:612–615.

Tristani-Firouzi, M., J. Chen, and M.C. Sanguinetti. 2002. Interactions between S4-S5 linker and S6 transmembrane domain modulate gating of HERG K+ channels. *J. Biol. Chem.* 277:18994–19000.

VanDongen, A.M.J., G.C. Frech, J.A. Drewe, R.H. Joho, and A.M. Brown. 1990. Alteration and restoration of K^+ channel function by deletions at the N- and C-termini. *Neuron.* 5:433–443.

Yang, J., Y.N. Jan, and L.Y. Jan. 1995. Determination of the subunit stoichiometry of an inward rectifying potassium channel. *Neuron.* 15:1441–1447.

Yang, N., A.L.J. George, and R. Horn. 1996. Molecular basis of charge movement in voltage-gated sodium channels. *Neuron.* 16: 113–122.

Yang, N., and R. Horn. 1995. Evidence for voltage-dependent S4 movement in sodium channels. *Neuron.* 15:213–218.

Zagotta, W.N., T. Hoshi, and R.W. Aldrich. 1994. Shaker potassium channel gating. III: Evaluation of kinetic models for activation. *J. Gen. Physiol.* 103:321–362.

Zheng, J., and F.J. Sigworth. 1997. Selectivity changes during activation of mutant Shaker potassium channels. *J. Gen. Physiol.* 110: 101–117.

Zhou, Y., J.H. Morais-Cabral, and R. MacKinnon. 2001. Chemistry of ion coordination and hydration revealed by a K^+ channel-Fab complex at 2.0 A resolution. *Nature.* 414:43–48.